Auxiliary material for "Strong decay of steep swells observed across oceans"

Fabrice Ardhuin[1*], Fabrice Collard[3], and Bertrand Chapron[2],

[1]Service Hydrographique et Ocanographique de la Marine, 29609 Brest, France
[2]Laboratoire d'Océanographie Spatiale, Ifremer,
Centre de Brest, 29280 Plouzané, France
[3]BOOST-Technologies, 29280 Plouzané, France

*To whom correspondence should be addressed; E-mail: ardhuin@shom.fr.

Discussion 1. Swell dissipation in existing numerical wave models

Another approach to the estimation of swell evolution is indirect, and uses numerical wave models. Following Tolman [3], and using recent observations of wave breaking statistics, one can get a quantitative estimate of the expected swell dissipation by removing the dissipation for all the wave components that are not expected to be directly affected by breaking. Based on the observations of [4] and [5], one can use the saturation spectrum

$$B\left(f\right)=2\pi\int_{0}^{2\pi}k^{3}F(f,\theta)/C_{g}\mathrm{d}\theta, \tag{1}$$

to define a threshold $B(f)=0.0012$ [6] below which no wave with a similar frequency is observed to break. Allowing for a margin of error, we have re-ran the model (fully described in Discussion 4) with the dissipation set to zero at all wave frequencies for which $B<0.001$. Because the wave heights are underestimated in the strong swell generation areas at mid-latitudes, the result in figure 1 can be interpreted as a lower bound for the wave overestimation in the absence of swell dissipation.

In the new parameterization used below, as was the case in the work of [3], the swell dissipation is specific, and the result without swell dissipation is easily obtained by setting the swell dissipation factor f_e to zero. In that case, because the wave heights are overestimated in the strong swell generation areas at mid-latitudes, we get an upper bound for the bias in the model without swell dissipation. In such model calculations the excess of energy in the swell band is limited by nonlinear interactions that are stronger for these steep non-dissipated swells than for

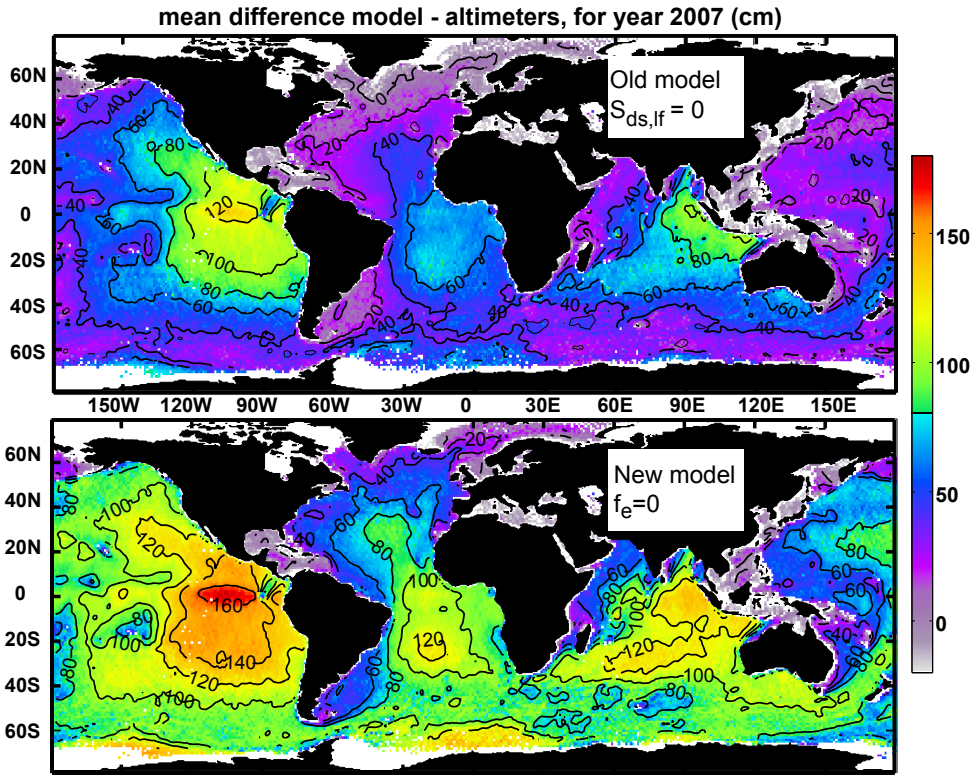

Figure 1: Mean difference between modelled without swell dissipation and observed wave heights for the year 2007. Observations combine of data from JASON, ENVISAT and GEOSAT-Follow On (GFO) altimeters, with a method described in [1]. Results are provided for (a) the parameterization by Bidlot et al. [2], (b) the new parameterization described below, except that in each model the swell dissipation was de-activated.

the real swells. Such a model study for the year 2007 show that in the absence of swell dissipation, wave heights are overestimated by 46 to 83 cm when averaged over the world ocean, which amounts to 24 to 44% of the average observed wave height. The large uncertainty in these estimates arises from the uncertainty in the initial wave generation as discussed by [7].

Any attempt to quantify swell dissipation with this type of indirect modelling approach, even when using complex data assimilation methods[8], is thus fundamentally limited by the many assumptions made in numerical wave models about other processes.

Methods. SAR database generation

In a first filtering procedure, only SAR swell partitions with peak wavelength and direction within 50 m and 20 degrees of expected were retained. We selected 12 storms with enough

SAR measurements along swell tracks, away from all islands. For each track of each of these storms, a short ASCII file was created containing one line for each SAR observation indicating distance from storm, time, position, swell partition observed wave height, wavelength and direction, direction mismatch from trajectories and local SAR derived wind speed. These files are available via anonymous ftp at the address `ftp.ifremer.fr` under the directory `ifremer/cersat/products/gridded/wavewatch3/HINDCAST/SWAO/`. All the analysis is based on these files only, with further filtering described below.

Swell track combination and SAR data selection

A typical track file contains 3 to 20 SAR data. In order to define a reliable attenuation of the swell energy, tracks with neighbouring values of the outgoing direction θ_0 are merged in relatively narrow direction bands, of the order of 5 to 10° (table 1), so that the combined wave properties are similar enough.

Because we need enough SAR data at large distance from the storm to allow for a reliable estimation of the swell attenuation, we ended up with only 32 track ensembles. These ensembles include a total of 149 tracks out of the 1245 in the original database. In each ensemble of swell tracks, some SAR data was filtered out based on the following criteria

- the distance from the source should be more than 4000 km, in order to satisfy the point source hypothesis which gives a reference wave height decay to which observed decay is compared to estimate the attenuation, and also to minimize errors due to the source localization.

- the wind speed should be more than 3 m s^{-1} and less than 13 m s^{-1}: this filters out weak wind conditions in which the waves are poorly imaged by the SAR, and high wind conditions in which the azimuthal cut-off may contaminate the swell height estimation, and generally increases the SAR error.

- the significant swell height H_{ss}, after bias correction based on the error model, should be more that 0.5 m. This makes sure that the signal to noise ratio in the image is large enough so that the wave height estimation is accurate enough.

- The selected data should span a range of distances from the source larger than 2000 km, in order to be representative of various locations along the track.

- The selected data should contain 6 or more SAR measurements, in order to provide a reliable swell dissipation estimate.

Eventually, 3 of the 32 track ensembles gave no reliable estimate of the swell attenuation because no SAR data matched all four criteria, thus table 1 and 2 only gives information on 29 track ensembles.

number	Storm time	Latitude	Longitude	T	$\theta_{\min}$	$\theta_{\max}$	N
1	20040216 00	160 E	37 N	14	76	85	35
2	20040216 00	160 E	37 N	15	85	95	26
3	20040216 00	160 E	37 N	16	75	85	6
4	20040418 18	165 E	52 S	14	63	94	11
5	20040418 18	165 E	52 S	15	85	90	17
6	20040418 18	165 E	52 S	16	77	88	35
7	20040418 18	165 E	52 S	17	75	85	32
8	20040630 23	145 E	25 N	13	75	80	23
9	20040709 18	177 W	55 S	14	32	37	11
10	20051021 00	155 W	50 N	15	120	130	23
11	20051021 00	155 W	50 N	17	135	150	30
12	20051114 03	160 E	40 N	13	90	100	21
13	20051113 12	160 E	40 N	15	85	95	49
14	20051113 12	160 E	40 N	17	80	90	24
15	20060310 00	137 E	45 N	16	140	150	19
16	20060310 12	136 E	45 N	14	145	155	13
17	20060310 23	136 E	45 N	13	130	140	10
18	20060427 00	155 E	54 S	15	65	75	47
19	20060427 06	150 E	58 S	14	65	75	44
20	20060427 06	143 E	53 S	16	35	45	16
21	20060427 06	140 E	53 S	17	35	45	19
22	20070212 18	168 E	38 N	15	74	90	48
23	20070324 00	165 W	53 S	15	85	90	15
24	20070324 00	165 W	53 S	17	77	82	11
25	20070324 00	165 W	53 S	18	71	73	17
26	20070812 00	100 W	55 S	15	-30	-24	19
27	20070812 00	100 W	55 S	17	-27	-17	14
28	20070812 00	100 W	55 S	18	-27	-17	8
29	20071030 00	155 W	47 S	15	75	90	62
Units	date and hour UTC	deg.	deg.	s	deg.	deg.	

Table 1: Ensembles of swell tracks selected for swell attenuation analysis. Each ensemble is defined by the source storm, the minimum and maximum outgoing directions $\theta_{\min}$ and $\theta_{\max}$. The number of SAR data that was retained for the estimation of the attenuation is N. All storms are located in the Pacific Ocean.

number	α	α_1	α_2	H	ε_1	Re_s	$f_{e,s}$	f_e	ε_2	U_{10}
1	26.3	22.3	29.3	5.6	8	10.1	0.0161	0.0129	13	6.2
2	22.1	16.1	25.9	4.0	17	4.8	0.0201	0.0137	17	6.4
3	9.4	-0.1	20.3	3.8	7	4.1	0.0082	0.0082	7	7.0
4	17.8	3.6	36.6	3.3	14	3.5	0.0136	0.0091	13	6.0
5	6.1	-8.0	16.8	2.4	9	1.7	0.0052	0.0035	9	6.5
6	12.0	5.3	18.3	3.0	14	2.5	0.0136	0.0092	13	7.6
7	8.7	2.7	15.1	2.8	11	2.1	0.0146	0.0098	11	7.4
8	11.5	2.5	18.6	2.0	25	1.4	0.0197	0.0064	25	5.1
9	13.3	-6.5	24.4	2.2	10	1.6	0.0039	0.0066	10	5.7
10	12.8	7.5	15.1	3.0	7	2.7	0.0134	0.0110	9	7.7
11	7.0	2.6	10.2	2.6	21	1.8	0.0631	0.0178	19	9.2
12	16.3	-1.2	39.8	2.3	13	1.8	0.0217	0.0088	13	7.9
13	11.9	4.8	13.8	2.4	17	1.7	0.0152	0.0146	17	6.5
14	1.4	-5.8	6.2	2.3	12	1.4	0.0021	0.0013	12	6.2
15	3.9	0.0	9.6	2.3	9	1.5	0.0045	0.0029	9	6.5
16	12.1	4.1	16.2	2.0	7	1.3	0.0293	0.0083	7	7.3
17	11.8	-1.4	19.3	1.8	9	1.1	-0.0022	0.0076	9	7.5
18	10.1	5.8	13.3	3.5	10	3.7	0.0065	0.0045	10	6.7
19	15.4	9.2	22.2	3.5	8	3.9	0.0091	0.0060	8	7.1
20	9.9	-1.2	18.5	2.9	6	2.4	0.0096	0.0064	6	5.7
21	6.2	-12.0	30.5	2.2	13	1.3	0.0327	0.0109	13	5.8
22	37.4	31.5	40.2	4.6	10	6.3	0.0334	0.0238	11	7.0
23	21.6	10.7	30.4	3.0	14	2.7	0.0284	0.0156	14	9.1
24	20.7	-5.2	41.1	2.5	11	1.6	0.0641	0.0215	11	9.8
25	6.0	-11.1	13.5	1.6	8	0.6	N.A.	N.A.	8	8.6
26	0.6	-6.7	2.4	1.5	11	0.7	N.A.	N.A.	11	6.1
27	0.4	-9.7	3.5	1.3	12	0.4	N.A.	N.A.	12	6.8
28	-5.9	-13.0	3.0	1.0	20	0.2	N.A.	N.A.	19	7.5
29	18.6	13.4	25.9	2.5	13	1.9	0.0380	0.0152	12	7.3
Units	10^{-8} m^{-1}	10^{-8} m^{-1}	10^{-8} m^{-1}	m	%	10^5			%	m s^{-1}

Table 2: Swell dissipation estimates. The fitted wave height at 4000 km from the source and constant linear decay coefficients are H and α, with ε_1 the mismatch of the linear attenuation to the observed wave heights, normalized by the r.m.s. observed height. The analysis was repeated 400 times using a Monte Carlo simulation of observation errors. The 16% and 84% levels in the estimation of α are given by α_1 and α_2. The fitted swell dissipation factor and total dissipation factor are $f_{e,s}$ and f_e, the latter with a relative error ε_2. Finally the mean wind speed over the SAR images used in the fit is also given by U_{10}, and the significant swell Reynolds number Re_s is estimated at 4000 km based on the linear fit.

Estimation of dissipation coefficients

For each set of SAR data, a function $H'_{ss}(\varphi)$ was fitted. Three fits were performed, one with a constant linear decay α, the others with constant dissipation factors $f_{e,s}$ or f_e. In each case the parameter α, f_e or $f_{e,s}$ was fitted together with the height $H_{ss}(\varphi_0)$ at a distance $x_0 = R\varphi_0 = 4000$ km from the storm source.

In practice, we scanned the possible values of $H_{ss}(\varphi_0)$, from 1 to 12 m, and α or f_e/$f_{e,s}$ (from -2.0×10^{-7} to 1×10^{-6} m^{-1} and -0.1 to 0.4, respectively), and the pair ($H_{ss}(\varphi_0)$,α), ($H'_{ss}(\varphi_0)$, $f_{e,s}$), or ($H''_{ss}(\varphi_0)$, f_e) that gave the minimum root mean square difference with observations $H_{ss}(\varphi_i)$ was retained (table 2).

In order to perform this fit, the function $H_{ss}(\varphi)$, was obtained from a numerical integration of

$$\frac{\mathrm{d}F\left(f,\theta,\varphi\right)}{\mathrm{d}\varphi} = \alpha R F((f,\theta),\varphi) \tag{2}$$

or

$$\begin{aligned} \frac{\mathrm{d}F\left(f,\theta,\varphi\right)}{\mathrm{d}\varphi} &= 16\frac{\rho_a}{\rho_w}\left(f_{\mathrm{e,s}} \quad \text{or} \quad \gamma f_{\mathrm{e}}\right)\frac{32\pi^4}{gT^4}R\sqrt{E_s}F\left(f,\theta,\varphi\right) \\ &\qquad \text{if} \quad \mathrm{Re_s} > 28000 \quad \text{or} \quad \mathrm{Re} > 100000 \\ \frac{\mathrm{d}F(f,\theta,\varphi)}{\mathrm{d}\varphi} &= \alpha_v R F\left(f,\theta,\varphi\right) \quad \text{otherwise,} \end{aligned} \tag{3}$$

where γ is $\max\{1.5, u_{\mathrm{orb}}/u_{\mathrm{orb,s}}\}$, in which the minimum value of 1.5 is meant to correct for the systematic underestimation of the large swells wave heights by the numerical model.

Numerical integrations were performed from $x = 4000$ to $x = 15000$ km, for each pair, e.g. (H, α), using a simple first order Euler scheme that was found to converge fast enough. Here the swell Reynolds number is defined as $\mathrm{Re}_s = 4u_{\mathrm{orb},s}a_{\mathrm{orb},s}/\nu$. The wind sea and other swell systems are taken into account in the f_e fits via the γ factor. The error function was computed by linearly interpolating the discretized $H'_s(\varphi_j)$ at the positions φ_i where selected observations were made.

In order to take into account the uncertainty of the SAR-derived wave heights, the estimation of α was repeated 400 times using uncorrelated random values of each SAR measurement, using the error model (section 2 of the paper). This Monte-Carlo estimation gave 400 values of α and H. The values corresponding to the 16 and 84 percentiles (this would correspond to one standard deviation if the values were Gaussian), are given in table 2 and shown as error bars on figure 2 of the paper.

The estimated swell dissipation coefficient α was found to be weakly sensitive to the exact choice of the distance x_0 and the minimum and maximum values for the wind speed and wave height. The variability of values of α for any range of wave slope is limited, and the confidence intervals of most of the estimates are relatively narrow. This suggests that our analysis is more accurate than previous studies, in which attenuations less than 1.0×10^{-7} m^{-1} were not reliable (this value corresponds to 0.05 dB/degree in [9]). This was likely due to the misalignement

of swell tracks with fixed measuring stations, and errors introduced by corrections for islands, problems that are absent in our dataset.

On the contrary, the estimation of f_e is limited by the known biasses of the model described below, used to estimate the significant surface orbital velocity amplitude $u_{\rm orb}$. Indeed, $u_{\rm orb} = 2\pi H_s/T_{m02}$, and although both H_s and T_{m02} are accurately estimated for average sea states, up to $H_s = 8$ m, there is a strong negative bias on wave heights in big storms, (for $H_s > 10$ m the bias is of the order of 10 to 15% of the value[10]), which is typical of conditions found in some cases here. We have thus corrected $u_{\rm orb}$ values from the model to be at least 1.5 times the SAR-derived swell orbital velocity $u_{\rm orb,s}$. The values of f_e are thus indicative, and are not expected to be accurate to better than 50%.

Discussion 2. Verification of geometrical optics asymptotes and point source hypothesis

The asymptotic energy-conserving solution $E \propto 1/\left[\varphi \sin(\varphi)\right]$ was verified using a semi-analytic model. This model uses the conservation of the spectral density along geodesics, which are computed analytically on the spherical Earth. At time $t = 0$ the initial wave spectra are prescribed to vary in space with a Gaussian storm distribution centered on the equator, with a width σ_x. At each position, the initial wave spectrum is prescribed to be a JONSWAP-type spectrum with a peak enhancement factor γ_J, which is related to a spectral width parameter σ_f[11]. Finally, the initial spectra are taken isotropic in directions. That latter aspect is not very realistic but simplifies the calculations since the initial spectral density is only given by the frequency and not the direction.

A space-time swell track is defined by the successive positions of an idealized wave packet travelling from the storm center at time $t = 0$ to a distance of 15000 km along the equator. At regular interval along this track, the wave spectrum is estimated by computing the spectral densities at a relative frequency resolution of 2% and a directional resolution of 0.5°. The quasi-analytic total wave energy is then obtained by summation over the spectrum, and compared to the asymptotic value.

The spatial decay of waves from such storms is thus completely specified by σ_x and γ_J. Due to the finite size of the storm source, the asymptotic decay should be attained in the limit $x \gg \sigma_x$. Further, the dispersive decay requires a finite width of the wave spectrum but it is also affected by the size of the source. Indeed, the dispersive spreading induces travel distance differences of the order of $\delta_x = x\sigma_f(\partial C_g/\partial f)/C_g$. This corresponds to a difference δ_x in the initial wave packet position at time $t = x/C_g$. The asymptotic decay is reached for $\delta_x \gg \sigma_x$.

In practice, for a peak period of 14 s, beyond 4000 km from the source and for a large storm with $\sigma_x = 550$ km, the error relative to the asymptotic decay is less than 0.4% for a Pierson-Moskowitz[12] spectrum (defined by $\gamma_J = 1$, which corresponds to a large σ_f), and 4.5% for a JONSWAP spectrum (defined by $\gamma_J = 3.3$, which corresponds to a small σ_f). These two spectra correspond the extremes of broad and narrow spectra in the open ocean,

with the JONSWAP form being rather rare and corresponding more to a coastal or enclosed sea situation. For a very compact storm, with $\sigma_x = 220$ km the maximum error is 1.2% for a Pierson-Moskowitz spectrum and up to 9.6% (negative bias) for JONSWAP spectrum. Thus very compact storms with young waves may lead to a significant departure from the generic decay asymptote. however, such an extreme deviation is still several times smaller than the differences between observed decays and the conservative asymptotic decay. Any error, in the source location also gives an error proportional to the position mismatch divided by the distance from the source, and this effect is expected to be negligible.

These calculations were done for fixed storms. The reader is referred to [13, 9], for a discussion of the effects of storm motion, that are likewise negligible. Thus, beyond 4000 km from the storm center, $E(\varphi)$ is not expected to deviate by more than 10% from the $1/\left[\varphi \sin(\varphi)\right]$ asymptote for realistic storm sizes and spectral widths.

Discussion 3. Boundary layer theory

For the sake of simplicity we will consider here the case of monochromatic waves propagating in the x direction only, and we will neglect the curvature of the surface. For the small steepness swells considered here that latter approximation is well founded and a more complete analysis can be found in [14]. Because the boundary layer is expected to be very thin compared to the wavelength, one can consider a local section of that boundary layer, for a given swell phase. The free stream velocity above the waves, just outside of the boundary layer is $u_+(x,t) = -\sigma a \cos(kx - \sigma t)$, where a is the swell amplitude and $\sigma = 2\pi/T$ is the radian frequency. The sub-surface velocity is $u_-(x,t) = \sigma a \cos(kx - \sigma t)$ (figure 2). Due to the oscillations that propagate at the phase velocity C, the horizontal advection of any quantity X by the flow velocity u, given by $u\partial X/\partial x$, can be neglected compared to its rate of change in time $\partial X/\partial t$ since the latter is a factor u/C smaller than the former, which is typically less that 0.1 for the swells considered here. Defining $\widetilde{u}(x,z,t) = \langle u(x,z,t)\rangle - u_-(x,t)$, where the brackets denote an average over the wave phase, the horizontal momentum equation is thus approximated by,

$$\frac{\partial \widetilde{u}}{\partial t} = -\frac{1}{\rho_a}\frac{\partial p}{\partial x} - \frac{\partial u_-}{\partial t} + G \tag{4}$$

where G represents the divergence of the vertical viscous and turbulent fluxes of horizontal momentum,

$$G = \nu \frac{\partial^2 \widetilde{u}}{\partial z^2} + \frac{\partial \left\langle u'w'\right\rangle}{\partial z}. \tag{5}$$

Because the boundary layer thickness δ is small compared to the wavelength, the pressure gradient in the boundary layer is given by the pressure gradient above the boundary layer, in balance with the horizontal acceleration, which is another way to write Bernoulli's equation[15], i.e. $-\partial p/\partial x/\rho_a = -\sigma^2 a \sin(kx - \sigma t) = \partial u_+/\partial t$. This yields

$$\frac{\partial \widetilde{u}}{\partial t} = 2\frac{\partial u_+}{\partial t} + G \tag{6}$$

with the boundary condition for $z \gg \delta$, $\widetilde{u}$ goes to $2u_+(x,t)$. The equation for the horizontal momentum is thus exactly identical to the one for the oscillatory boundary layer over a fixed bottom with wave of the same period but with an amplitude twice as large. In the viscous case, one recovers, after some straightforward algebra, the known viscous result, i.e., for $z > \zeta$,

$$\widetilde{u}(x,z,t) = 2\sigma a \left[\mathrm{e}^{z_+} \cos\left(kx - \sigma t + z_+\right) - \cos\left(kx - \sigma t\right)\right] + O(\rho_a/\rho_w) \tag{7}$$

where $z_+ = (z-\zeta)/\sqrt{2\nu/\sigma}$, with the surface elevation $\zeta(x,t) = a\cos(kx - \sigma t)$. Evaluating the work of the viscous stresses $\langle \rho_a \nu u \partial u/\partial z \rangle$, eq. (7) gives the low frequency asymptote to the viscous decay coefficient, $\alpha_v = 2k\sqrt{2\nu\sigma}\rho_a/\rho_w/C_g$. This result was previously obtained using a Lagrangian approach without all the above simplifying assumptions[16]. The full viscous result is obtained by also considering the water viscosity ν_w, which gives the $O(\rho_a/\rho_w)$ correction for the motion in the air, and the classical dissipation term with a decay $\alpha_{vw} = 4k^2\nu_w/C_g$, which dominates for the short gravity waves.

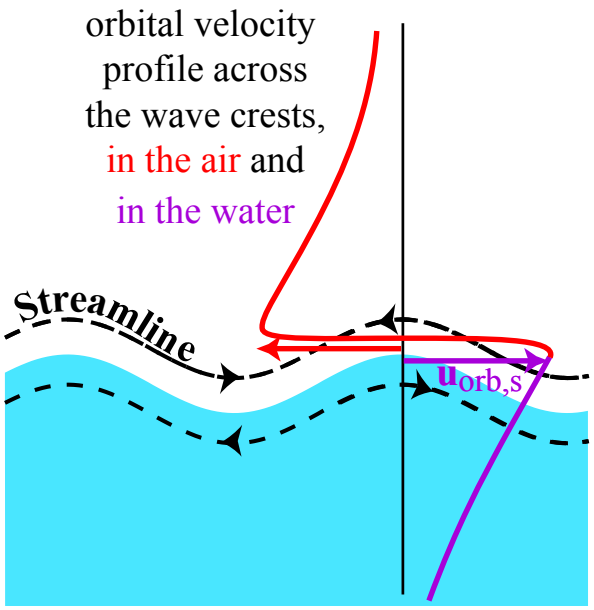

Figure 2: Boundary layer over waves in the absence of wind. Because of the larger inertia of the water compared to the air, most of the adjustment from the sub-surface velocity to the free stream velocity in the air occurs on the air-side of the surface.

As a result, for a comparison with fixed bottom boundary layers, the Reynolds number based on the orbital motion should be redefined with a doubled velocity and a doubled displacement, i.e. Re$= 4u_{\mathrm{orb}}a_{\mathrm{orb}}/\nu$. For monochromatic waves $a_{\mathrm{orb}} = a$ and $u_{\mathrm{orb}} = a\sigma = 2\pi a/T$. For random waves, investigations of the ocean bottom boundary layer suggest that the boundary layer properties are roughly equivalent to that of a monochromatic boundary layer defined by significant properties[17].

Although the wind was neglected here, it should influence the shear stresses when its vertical shear is of the order of the wave-induced shear. Taking a boundary layer thickness δ and wind friction velocity $u_\star$, and assuming a logarithmic wind profile, this should occur when $u_\star/(\kappa\delta)$ exceeds $2u_{\rm orb}/\delta$, where κ is von Kármán's constant. This corresponds to, roughly, $u_\star > u_{\rm orb}$. For swells with T < 15 s and $H_{ss} > 2$ m (i.e. $u_{\rm orb,s} > 0.4$ m s^{-1}), and winds less than 7 m s^{-1} (i.e. $u_\star < 0.2$ m s^{-1}), the wind effect on f_e may be small and the previous analysis is likely valid. In general, however, the nonlinear interaction of the wave motion and wind should be considered, which requires an extension of existing theories for the distortion of the airflow to finite swell amplitudes.

Discussion 4. Improvement in numerical wave modelling based on the present analysis

Model description

A preliminary validation of a new wave model parameterization has been performed using the present results. Although relatively few tests have been carried out, one of the parameterizations turned out to outperform today's best wave models by a significant margin. This parameterization was thus implemented in the wave model routinely used at SHOM as part of the Previmer project, providing wave information to a variety of users (`http://www.previmer.org`), with validation reported monthly to the Joint Commission on Marine Meteorology wave model verification project (http://www.jcomm-services.org/Wave-Forecast-Verification-Project.html).

The results discussed below do not constitute any proof of the correctness of the wave attenuation mechanism highlighted here, but rather gives an indication on the usefulness of this result. Further, they provide an order of magnitude of the effect on the entire sea state, beyond the few swell partitions studied above. In order to highlight this magnitude, the model was ran with three constant values of the dissipation factor f_e (0, 0.0035 and 0.0070). Another run was performed with an adjusted function form for the dependence of f_e on the wind speed and direction, as explained below. This adjusted model was used in figures 1 and 2.

Wave models are by no means perfect. They predict the wave spectrum based on the wave action balance equation[18], which, in deep water and without current, is

$$\frac{{\rm d}F(f,\theta)}{{\rm d}t} = S_{\rm in}(f,\theta) + S_{\rm nl}(f,\theta) + S_{\rm ds}(f,\theta), \tag{8}$$

where the spectrum F and source terms S are also functions of the geographical position, omitted here for simplicity. Solving that equation presents a number of challenges. First of all, the wind-wave generation $S_{\rm in}$ and wave dissipation terms $S_{\rm ds}$ are poorly known. Second, the better known non-linear interaction term $S_{\rm nl}(f,\theta)$ requires extensive computer power that make routine wave forecasting barely feasible today. That term is thus usually parameterized with the approximate form $S_{\rm nl}^{\rm DIA}$[19]. Using that term may compensate for errors in the other two[20, 21]

but the source terms are essentially uncertain in active wind wave generation conditions, and their numerical integration in time is not simple either[22]. Finally, the integration of the wave action balance requires accurate numerical schemes when swells are to be propagated across ocean basins[23].

In previous work, it was found that the input term by Janssen[24], used in the WAM-Cycle 4 model, probably has the right order of magnitude[25, 21]. On top of this term, we now add a "wind output" term in order to represent the upward momentum flux associated with the wave attenuation observed here. If Re$<$100000 This term takes the form

$$S_{\mathrm{out}}\left(f,\theta\right)=-\frac{\rho_a}{\rho_w}\left\{2k\sqrt{2\nu\sigma}\right\}F\left(f,\theta\right). \tag{9}$$

and otherwise

$$S_{\mathrm{out}}\left(f,\theta\right)=-\frac{\rho_a}{\rho_w}\left\{16f_e\sigma^2u_{\mathrm{orb}}/g\right\}F\left(f,\theta\right), \tag{10}$$

The first equation is the linear viscous decay[26], and the second term is a parameterization for the nonlinear turbulent decay. When comparing model results to observations, it was found that the model tended to underestimate large swells and overestimate small swells, with regional biasses. This defect is likely due, in part, to errors in the generation or non-linear evolution of theses swells. However, it was chosen to adjust f_e as a function of the wind speed and direction,

$$f_e=0.7f_{e,GM}+\left[0.015-0.018\cos(\theta-\theta_u)\right]u_\star/u_{\mathrm{orb}}, \tag{11}$$

where $f_{e,GM}$ is the friction factor given by Grant and Madsen's (1979) theory for rough oscillatory boundary layers without a mean flow, using a roughness length adjusted to 0.04 times the roughness for the wind. This gives a stronger dissipation for swells opposed to winds.

Thus the full wind-wave interaction source term reads

$$S_{\mathrm{in}}\left(f,\theta\right)=\frac{\rho_a}{\rho_w}\frac{\beta_{\max}}{\kappa^2}\mathrm{e}^ZZ^4\left(\frac{u_\star}{C}+z_\alpha\right)^2\cos^2(\theta-\theta_u)\sigma F\left(f,\theta\right)+S_{\mathrm{out}}\left(f,\theta\right), \tag{12}$$

where $\beta_{\max}$ is (constant) a non-dimensional growth parameter, κ is von Kármán's constant. In the present implementation the air/water density ratio is constant. We define $Z=\log(\mu)$ where μ is given by Janssen (1991, eq. 16), and corrected for intermediate water depths, so that

$$Z=\log(kz_1)+\kappa/\left[\cos\left(\theta-\theta_u\right)\left(u_\star^{\prime}C+z_\alpha\right)\right], \tag{13}$$

where z_1 is a roughness length modified by the wave-supported stress τ_w, and z_α is a wave age tuning parameter.

The effective roughness z_1 is implicitly defined by

$$U_{10} = \frac{u_\star}{\kappa}\log\left(\frac{10\ \mathrm{m}}{z_1}\right) \tag{14}$$

$$z_0 = \max\left\{\alpha_0\frac{u_\star^2}{g},0.0020\right\} \tag{15}$$

$$z_1 = \frac{z_0}{\sqrt{1-\tau_w/\tau}}. \tag{16}$$

The maximum value of z_0 was added to reduce the unrealistic stresses at high winds that are otherwise given by the standard parameterization. This is equivalent to setting a maximum wind drag coefficient of 2.8×10^{-3}. This, together with the different value of p and the use of an effective friction velocity $u'_\star(f)$ instead of $u_\star$ in (13) are the only changes to the general form of Janssen's[24] wind input. That friction velocity is defined by

$$\left(u'_\star(f)\right)^2 = \left| u_\star^2 \left(\cos\theta_u, \sin\theta_u\right) - |s_u| \int_0^f \int_0^{2\pi} \frac{S_{in}\left(f', \theta'\right)}{C} \left(\cos\theta, \sin\theta\right) \mathrm{d}f' \mathrm{d}\theta', \right| . \tag{17}$$

As for the dissipation, most previously proposed parameterizations dissipate swells with the same formulation that is used for wave breaking, an approach which is clearly not supported by the present observations nor by the wave breaking statistics analyzed by others[4]. We have thus chosen to use an a dissipation term, formulated in terms of the direction-integrated spectral saturation $B\left(f\right)$ given by eq. (1) [5] and a partially-integrated saturation,

$$B'\left(f, \theta\right) = 2\pi \int_{\theta-\Delta\theta}^{\theta+\Delta\theta} k^3 F(f, \theta')/C_g \mathrm{d}\theta', \tag{18}$$

to give,

$$\begin{aligned} S_{\mathrm{ds}}(f, \theta) = \sigma C_{\mathrm{ds}} \Bigg\{ \delta \left[\max\left\{ \frac{B\left(f\right)}{B_r} - 1, 0 \right\} \right]^2 \\ + (1-\delta) \left[\max\left\{ \frac{B'\left(f, \theta\right)}{B_r} - 1, 0 \right\} \right]^2 \Bigg\} F(f, \theta). \end{aligned} \tag{19}$$

with a realistic threshold $B_r = 1.2 \times 10^{-3}$ corresponding to the onset of wave breaking[6]. It is important to note that this dissipation term does not affect swells, which are not steep enough to break, except in very strong adverse currents or in very shallow water.

The dissipation parameters $C_{\mathrm{ds}} = -2.4 \times 10^{-5}$, $\Delta\theta = 70^\circ$ and $\delta = 0.25$ have been adjusted to the directional short fetch measurements of Ardhuin et al. (2007), together with the wind input parameters $\beta_{\max} = 1.75$, and the wave age correction factor $z_\alpha = 0.005$, instead of the values 1.2 and 0.011 typically used[2].

The model used to integrate the source term balance is the version 3.14 of WAVEWATCH III[28], with the modifications discussed here. The model was ran for the entire year 2006 with wind and sea ice concentration analyses from ECMWF (the sea ice data actually orginates from NOAA). The model grid resolution is 0.5 degree in latitude and longitude and the spectral discretization uses 24 directions and 32 frequencies exponentially spaced from 0.037 Hz to 0.07 Hz.

This model was ran with four values of the swell friction factor f_e, namely 0.0, 0.0035, 0.007, and the functional form of eq. (11). All other parameters were kept unchanged. The model was also ran with the parameterization used operationally at ECMWF and called here "BAJ"[2], in which $\beta_{\max}$ was increased to from 1.2 to 1.25, in order to reduce a bias likely due to differences in numerical schemes and spatial resolutions between in the ECWAM model used at ECMWF and the WAVEWATCH III model used here.

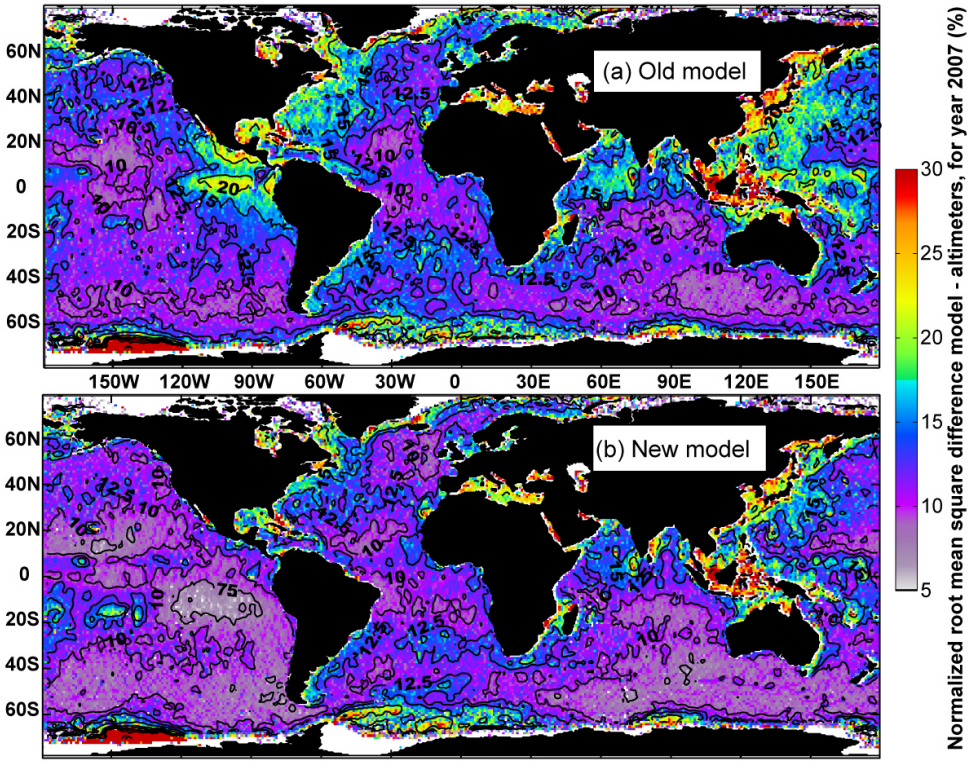

Figure 3: Normalized root mean square difference (NE), in percent, for H_s over the year 2007 between models and altimeter data from satellites JASON, GFO and ENVISAT. (a) the "old" model uses the BAJ parameterization[2] situ locations, and (b) the "new model" uses the parameterization proposed here with f_e given by eq. (13). The altimeter analysis method is detailed in Rascle et al. (2008).

Model results and discussion

Here we illustrate the model performance using altimeter-derived wave heights, and wave heights, and other parameters derived from in situ platforms collected as part of the IOC-WMO Joint Commission on Marine Meteorology (JCOMM) wave model comparison exercise[29]. Further data provided by the U.S. National Data Buoy Center are also used for representative buoys, designated here by their World Meteorological Organization (WMO) identification number

- 62163 : Offshore of Western France, North Atlantic. Large storms in winter and spring, some swells year round.
- 46001 : Offshore of Kodiak, AK. Large storms in winter, exposed to remote Pacific swells.

- 46005 : Offshore of Aberdeen, WA. Important storms in winter, well exposed to Pacific swells.
- 41001 : 300 km East of Cape Hateras, relatively short fetches from the West and exposed to westbound Atlantic swells.
- 46047 : Tanner Banks, CA. Swell-dominated conditions.
- 51001 : North-west of Kauai, HI. Swell-dominated conditions.
- 51028 : Christmas Island, on the Equator, south of Hawaii. That buoys is exposed to most Pacific swells, and has local wind seas generated by trade winds. Local currents can be significant, and typically range from 0.3 to 1 m/s. These currents are not included in the present calculations, but can have a large effect on waves[1].

Parameterizations that do not account for swell decay, including BAJ or the present parameterization with $f_e = 0$, give a large meridional gradient in wave height bias against altimeters, with a difference of about 50 cm in bias between the swell generation areas at mid-latitudes and the calm regions of the East Equatorial Pacific. A constant dissipation factor $f_e = 0.0035$ applied to the total orbital velocity is able to remove most of that gradient, as the swell attenuation from the source regions to their final destination is now reproduced. Further adjustment are now being considered [10].

The value $f_e = 0.0035$ yields smaller biasses against altimeter data, on average, and generally produces better correlation with buoy data, in terms of wave height (table 3), and energy at low frequencies (tables 4). However, in some locations, larger values of f_e provide a better agreement with observed low frequency energies (table 4). The model with $f_e = 0.0035$ is well calibrated for stormy regions, such as the North East Atlantic or the Gulf of Alaska, with still a little negative bias on wave heights. In that case, regions with more moderate wave climates have both understimated wave heights and overestimated mean periods, i.e. there is still too much swell arriving from storm areas but not enough local generation.

It appears likely that both swell generation and dissipation are stronger in reality than in the $f_e = 0.0035$ model runs. A full retuning of all model parameters, will likely be needed to further improve model results. Improvements are already obtained by introducing a small empirical wind correction in f_e, defined by eq. (11).

Some sea states are more sensitive to others to changes in the value of f_e. Not surprisingly, swell-dominated regions are extremely sensitive to the choice of f_e. For example, the model normalized bias for the wave height at buoy 51028 changes by 72 percentage points from +59 to -12% as f_e increases from 0 to 0.007 (table 3). The low-frequency wave energy is, obviously, even more sensitive to that parameter (table 4).

Buoy spectral wave data can be used effectively to discriminate between candidate parameterizations for the swell attenuation, in complement to a direct estimation of attenuation rates from spectral satellite data. The parameterizations with f_e depending on the wind speed through the surface roughness and a correction factor for the wind speed and direction (eq. 6) clearly

Model run	BAJ	f_e from (11)	$f_e = 0$	$f_e = 0.0035$	$f_e = 0.007$
62163 NE	10.6	**9.3**	17.0	10.1	16.3
62163 NB	-4.4	**-1.8**	13.4	-2.8	-11.4
62163 r	0.9810	**0.9842**	0.9781	0.9806	0.9723
46001 NE	10.7	**9.5**	22.7	**9.5**	13.2
46001 NB	-3.7	-0.9	19.6	**-0.5**	-8.1
46001 r	0.9737	**0.9765**	0.9674	0.9762	0.9714
46005 NE	12.3	**10.9**	33.1	11.5	16.3
46005 NB	**1.6**	3.0	30.9	1.7	-8.8
46005 r	0.9619	**0.9723**	0.9667	0.9666	0.9516
41001 NE	17.2	**15.4**	22.8	15.5	17.8
41001 NB	-9.7	-6.4	14.6	**-3.6**	-7.6
41001 r	0.9641	**0.9697**	0.9619	0.9673	0.9617
46047 NE	**14.5**	15.0	43.8	16.6	26.2
46047 NB	**-2.2**	-8.1	40.0	-7.9	-20.1
46047 r	0.9339	**0.9506**	0.8978	0.9433	0.9222
51001 NE	13.5	**11.9**	40.3	13.0	22.0
51001 NB	**-1.9**	-3.7	38.0	-3.9	-15.3
51001 r	0.9252	**0.9461**	0.9245	0.9374	0.9080
51028 NE	13.2	**12.1**	61.3	14.4	22.2
51028 NB	4.7	**-1.7**	59.9	-2.9	-12.7
51028 r	0.8062	**0.8757**	0.7928	0.7807	0.6134

Table 3: Model errors statistics on significant wave height for several model runs, at WMO buoys 62163, 65001, 41002, 51001, 65005, 46069 and 51028. NE stands for the r.m.s. error normalized by the r.m.s. observation, in %, NB stands for the bias normalized by the r.m.s. observation, in %, and r is Pearson's linear correlation coefficient. For each parameter the best model is highlighted in bold. Observed hourly spectral data was retrieved from the U.S. National Data Buoy Center historical data web site, and spectra were averaged over 3 hour intevals, every 3 hours. For buoy 62163, displayed but not archived by NDBC, real-time data was archived every hour and the wave heights were averaged over 3 hour intevals, every 3 hours.

Model run	BAJ	f_e from (11)	$f_e = 0$	$f_e = 0.0035$	$f_e = 0.007$
46001 NE	28.3	27.1	61.4	27.2	**24.0**
46001 NB	14.2	13.9	55.3	12.9	**-1.8**
46001 r	0.9437	**0.9497**	0.9325	0.9458	0.9456
46005 NE	34.7	32.6	73.5	31.0	**27.1**
46005 NB	22.2	21.1	69.1	18.5	**-2.9**
46005 r	0.9271	**0.9393**	0.9358	0.9353	0.9261
41001 NE	**34.5**	38.5	54.7	39.6	41.9
41001 NB	-2.8	-7.6	31.5	**-6.5**	-14.8
41001 r	0.9243	**0.9248**	0.8775	0.9164	0.9184
46047 NE	28.1	**22.3**	87.9	25.2	37.0
46047 NB	13.5	**5.9**	84.0	**5.9**	-21.6
46047 r	0.9038	**0.9266**	0.8833	0.9160	0.9047
51001 NE	29.3	**25.1**	63.8	25.9	31.1
51001 NB	12.0	**5.4**	58.1	5.5	-15.0
51001 r	0.9172	**0.9305**	0.9197	0.9259	0.9247
51028 NE	39.4	**28.2**	110.3	30.0	34.1
51028 NB	25.1	**8.5**	105.4	13.4	-19.0
51028 r	0.7786	0.8007	0.7891	0.8005	0.7874

Table 4: Like table 3, for the low frequency wave height (0.037–0.08 Hz).

provides a superior fit to most of the data. In particular the relative error against altimeter data averaged over the world ocean is of only 11.5% (figure 4)

Acknowledgments. This research would not have been possible without the wind and ice fields provided by ECMWF and Meteo-France, the satellite altimeter data provided by ESA and CNES, and the many in situ observations acquired by all contributors to the JCOMM (WMO-IOC) exchange program, including NOAA/NDBC, Meteo-France, Puertos del Estado, the U.K. Met. Office, the Australian Weather Bureau and the Irish Marine Institute. Finally, the quality of the present model and feasibility of our research owes much to the very kind help from H.L. Tolman (NOAA/NCEP) and Jean Bidlot and Peter Janssen (ECMWF) and anonymous reviewers. We are indebted to Denis Croizé-Fillon and Pierre Queffelou (Ifremer) who performed the comparison of model and altimeter data. This work was partially funded by the ANR project HEXECO and DGA funded project ECORS.

References

[1] N. Rascle, F. Ardhuin, P. Queffeulou, and D. Croizé-Fillon, "A global wave parameter database for geophysical applications. part 1: wave-current-turbulence interaction param-

eters for the open ocean based on traditional parameterizations," *Ocean Modelling*, 2008. doi:10.1016/j.ocemod.2008.07.006.

URL link.

[2] J. Bidlot, S. Abdalla, and P. Janssen, "A revised formulation for ocean wave dissipation in CY25R1," Tech. Rep. Memorandum R60.9/JB/0516, Research Department, ECMWF, Reading, U. K., 2005.

[3] H. L. Tolman, "Distributed memory concepts in the wave model WAVEWATCH III," *Parallel Computing*, vol. 28, pp. 35–52, 2002.

[4] M. L. Banner, A. V. Babanin, and I. R. Young, "Breaking probability for dominant waves on the sea surface," *J. Phys. Oceanogr.*, vol. 30, pp. 3145–3160, 2000.

URL link.

[5] M. L. Banner, J. R. Gemmrich, and D. M. Farmer, "Multiscale measurement of ocean wave breaking probability," *J. Phys. Oceanogr.*, vol. 32, pp. 3364–3374, 2002.

[6] A. V. Babanin and I. R. Young, "Two-phase behaviour of the spectral dissipation of wind waves," in *Proceedings of the 5th International Symposium Ocean Wave Measurement and Analysis, Madrid, june 2005*, ASCE, 2005. paper number 51.

[7] P. Heimbach and K. Hasselmann, "Development and application of satellite retrievals of ocean wave spectra," in *Satellites, oceanography and society* (D. Halpern, ed.), pp. 5–33, Elsevier, Amsterdam, 2000.

[8] E. Bauer, K. Hasselmann, I. R. Young, and S. Hasselmann, "Assimilation of wave data into the wave model WAM using an impulse response function method," *J. Geophys. Res.*, vol. 101, pp. 3801–3816, 1996.

[9] F. E. Snodgrass, G. W. Groves, K. Hasselmann, G. R. Miller, W. H. Munk, and W. H. Powers, "Propagation of ocean swell across the Pacific," *Phil. Trans. Roy. Soc. London*, vol. A249, pp. 431–497, 1966.

[10] F. Ardhuin, F. Collard, B. Chapron, P. Queffeulou, J.-F. Filipot, and M. Hamon, "Spectral wave dissipation based on observations: a global validation," in *Proceedings of Chinese-German Joint Symposium on Hydraulics and Ocean Engineering, Darmstadt, Germany*, 2008.

[11] K. Hasselmann, T. P. Barnett, E. Bouws, H. Carlson, D. E. Cartwright, K. Enke, J. A. Ewing, H. Gienapp, D. E. Hasselmann, P. Kruseman, A. Meerburg, P. Müller, D. J. Olbers, K. Richter, W. Sell, and H. Walden, "Measurements of wind-wave growth and swell decay during the Joint North Sea Wave Project," *Deut. Hydrogr. Z.*, vol. 8, no. 12, pp. 1–95, 1973. Suppl. A.

[12] W. J. Pierson, Jr and L. Moskowitz, "A proposed spectral form for fully developed wind seas based on the similarity theory of S. A. Kitaigorodskii," *J. Geophys. Res.*, vol. 69, pp. 5,181–5,190, Dec. 1964.

[13] W. H. Munk, G. R. Miller, F. E. Snodgrass, and N. F. Barber, "Directional recording of swell from distant storms," *Phil. Trans. Roy. Soc. London A*, vol. 255, pp. 505–584, 1963.

[14] V. N. Kudryavtsev and V. K. Makin, "Impact of swell on the marine atmospheric boundary layer," *J. Phys. Oceanogr.*, vol. 34, pp. 934–949, 2004.

[15] C. C. Mei, *Applied dynamics of ocean surface waves*. Singapore: World Scientific, second ed., 1989. 740 p.

[16] J. E. Weber and E. Førland, "Effect of the air on the drift velocity of water waves," *J. Fluid Mech.*, vol. 218, pp. 619–640, 1990.

[17] P. Traykovski, A. E. Hay, J. D. Irish, and J. F. Lynch, "Geometry, migration, and evolution of wave orbital ripples at LEO-15," *J. Geophys. Res.*, vol. 104, pp. 1,505–1,524, Jan. 1999.

[18] G. J. Komen, L. Cavaleri, M. Donelan, K. Hasselmann, S. Hasselmann, and P. A. E. M. Janssen, *Dynamics and modelling of ocean waves*. Cambridge: Cambridge University Press, 1994.

[19] S. Hasselmann, K. Hasselmann, J. Allender, and T. Barnett, "Computation and parameterizations of the nonlinear energy transfer in a gravity-wave spectrum. Part II: Parameterizations of the nonlinear energy transfer for application in wave models," *J. Phys. Oceanogr.*, vol. 15, pp. 1378–1391, 1985.

[20] M. L. Banner and I. R. Young, "Modeling spectral dissipation in the evolution of wind waves. part I: assessment of existing model performance," *J. Phys. Oceanogr.*, vol. 24, no. 7, pp. 1550–1570, 1994.

[21] F. Ardhuin, T. H. C. Herbers, K. P. Watts, G. P. van Vledder, R. Jensen, and H. Graber, "Swell and slanting fetch effects on wind wave growth," *J. Phys. Oceanogr.*, vol. 37, no. 4, pp. 908–931, 2007.

[22] J. C. Hargreaves and J. D. Annan, "Comments on improvement of the short-fetch behavior in the wave ocean model (WAM)," *J. Atmos. Ocean Technol.*, vol. 18, pp. 711–715, 2000. URL link.

[23] H. L. Tolman, "Alleviating the garden sprinkler effect in wind wave models," *Ocean Modelling*, vol. 4, pp. 269–289, 2002.

[24] P. A. E. M. Janssen, "Quasi-linear theory of of wind wave generation applied to wave forecasting," *J. Phys. Oceanogr.*, vol. 21, pp. 1631–1642, 1991. See comments by D. Chalikov, J. Phys. Oceanogr. 1993, vol. 23 pp. 1597-1600.

[25] M. L. Banner and R. P. Morison, "On modeling spectral dissipation due to wave breaking for ocean wind waves," in *Proceedings of the 9th International workshop on wave hindcasting and forecasting, Victoria, Canada*, 2006.

[26] B. D. Dore, "Some effects of the air-water interface on gravity waves," *Geophys. Astrophys. Fluid. Dyn.*, vol. 10, pp. 215–230, 1978.

[27] W. D. Grant and O. S. Madsen, "Combined wave and current interaction with a rough bottom," *J. Geophys. Res.*, vol. 84, pp. 1797–1808, 1979.

[28] H. L. Tolman, "The 2007 release of WAVEWATCH III," in *Proceedings, 10th Int. Workshop of Wave Hindcasting and Forecasting, Hawaii*, 2007.

URL link.

[29] J.-R. Bidlot, J.-G. Li, P. Wittmann, M. Fauchon, H. Chen, J. Lefèvre, T. Bruns, D. Greenslade, F. Ardhuin, N. Kohno, S. Park, and M. Gomez, "Inter-comparison of operational wave forecasting systems," in *Proceedings, 10th Int. WOrkshop of Wave Hindcasting and Forecasting, Hawaii*, 2007.

URL link.